Applied Catalysis B: Environmental 179 (2015) 412–421

Contents lists available at ScienceDirect

Applied Catalysis B: Environmental

journal homepage: www.elsevier.com/locate/apcatb

Promoting effect of trace Pd on hydrotalcite-derived Ni/Mg/Al catalyst in oxidative steam reforming of biomass tar

Jinhai Chen [a], Masazumi Tamura [a], Yoshinao Nakagawa [a], Kazu Okumura [b], Keiichi Tomishige [a,*]

[a] Department of Applied Chemistry, School of Engineering, Tohoku University, 6-6-07, Aoba, Aramaki, Aoba-ku, Sendai 980-8579, Japan
[b] Department of Applied Chemistry, Faculty of Engineering, Kogakuin University, 2665-1 Nakano-machi, Hachioji, Tokyo 192-0015, Japan

ARTICLE INFO

Article history:
Received 13 March 2015
Received in revised form 28 April 2015
Accepted 21 May 2015
Available online 22 May 2015

Keywords:
Oxidative steam reforming
Tar
Palladium
Nickel
Hydrotalcite

ABSTRACT

Promoting effects of trace noble metals (Pd, Pt, Au, Ru, Rh and Ir) on the activity and stability of the Ni catalyst prepared from the hydrotalcite-like compounds containing Ni, Mg, and Al were investigated in steam reforming and oxidative steam reforming of tar derived from pyrolysis of biomass. The optimum loading of Pd was 0.05 wt% (0.05PdNi catalyst; molar ratio of Pd/Ni = 0.0023), and this catalyst showed higher performance than the other noble-metal-added catalysts with the same noble metal/Ni molar ratio. Characterization results indicated that the addition of 0.05 wt% Pd enhanced the reducibility of Ni species and the dispersion of Ni metal particles simultaneously, which can be attributed to the highest catalytic performance. The monometallic Ni catalyst (0PdNi) totally lost the catalytic activity due to the oxidation of catalytically active Ni metal particles by oxygen after two hour stability test in oxidative steam reforming. In contrast, the oxidation of Ni metal particles did not occur on 0.05PdNi catalyst, and the 0.05PdNi catalyst showed stable catalytic performance during the two hour stability test, which can be due to the formation of highly dispersed Pd atoms on the surface of Ni metal particles on the 0.05PdNi catalyst as suggested by Pd *K*-edge EXAFS analysis.

1. Introduction

Gasification of biomass into syngas is expected to be used in various fields such as power generation and the production of hydrogen and liquid fuels through C1 chemistry (e.g., methanol and Fischer–Tropsch oil) [1–6]. Various methods for the conversion of biomass to syngas have been known and reviewed [1,2,5,6]. One of the methods is the combination of the pyrolysis of biomass and the subsequent catalytic steam reforming of the tar derived from the pyrolysis at low temperature. Here, this method is denoted as "pyrolysis + reforming". The merit of this pyrolysis + reforming is that the very high temperature needed in the case of non-catalytic steam gasification is not necessary [1,2]. In the pyrolysis + reforming method, one of the key points is the development of metal catalysts with high performance in the steam reforming of the tar from biomass pyrolysis, and the catalyst development has been summarized in reviews [7–9]. It has been reported that Ni or Co catalysts and the catalysts modified with various kinds of additives and supports are effective to the steam reforming of the tar and its model compounds [10–39]. One demerit of this pyrolysis + reforming is that external heat supply is required because the steam reforming of tar is a highly endothermic reaction. In the case of natural gas conversion technology, the steam reforming of methane has been shifted to the autothermal reforming of methane where oxygen is introduced to the reactor, and exothermic reaction of methane with oxygen is combined with the endothermic steam reforming of methane [40,41]. This enables the effective heat supply from the exothermic reaction to the endothermic reaction. Furthermore, the catalyst development for the introduction of oxygen together with methane and steam to the catalyst bed, which is denoted as oxidative steam reforming, has been attempted in order to suppress the hot spot formation at the catalyst bed inlet. The Ni catalyst effectively modified with small amount of suitable noble metals has been developed for this oxidative steam reforming of methane [42–51].

In the present study, we attempted the oxidative steam reforming of biomass tar, where oxygen is introduced to the catalyst bed together with steam and the tar from the pyrolysis of biomass. Besides, the presence of oxygen can significantly reduce the amount of the deposited coke on the catalysts surface, which is one of the main causes of catalyst deactivation [52–54]. Nickel based catalysts have been extensively studied in the pyrolysis + reforming

* Corresponding author. Tel.: +81 22 795 7214; fax: +81 22 795 7214.
E-mail address: tomi@erec.che.tohoku.ac.jp (K. Tomishige).

http://dx.doi.org/10.1016/j.apcatb.2015.05.042
0926-3373/

system for the conversion of biomass to syngas because of its high reforming activity and low cost [7,10–13,16,18,19,23,26,28–39,55]. However, Ni metal species can be oxidized by oxygen and lose their reforming activity in the oxidative steam reforming of biomass tar like the case of that of methane [46,51,56–58]. A possible method for the suppression of the oxidation of Ni metal species is the modification of Ni catalysts with a trace of noble metal. Modification of Ni catalyst for the steam reforming of methane with a trace of noble metal has been reported to be very effective to the enhancement of the catalyst reducibility [51].

Hydrotalcite-like compounds (HTlcs) are suitable precursors for preparing well-dispersed and thermally stable metal particles as active components for catalysts [59]. It has been reported that Ni/Mg/Al catalyst prepared by the calcination and reduction pretreatment of Ni-Mg-Al HTlcs has nanocomposite structure of Ni metal particles supported on Mg(Ni, Al)O (MgO-like phase containing Al and Ni) particles with a similar size to the Ni particles [60]. In particular, the nanocomposite structure can be connected to the high performance in the steam reforming of biomass tar [18,22,23,60]: high dispersion of Ni metal particles was maintained by the presence of Mg-Al-O mixed oxides among Ni metal particles [60]; the amount of coke was decreased by cohesive contact between Ni metal particles and the oxide particles [60]; Ni particles was re-dispersed by calcination–reduction process for regeneration [15,23]. Ni/Mg(Ni, Al)O catalysts also exhibited high stability at the steady operation in steam reforming of methane [61,62]. However, it was totally deactivated just after first steam purging in the daily start-up and shut-down operation (DSSO) because of the oxidation of Ni metal by steam. In contrast, dipping 0.05 wt% of Ru, Rh, and Pt and 0.1 wt% of Pd on Ni/Mg(Ni, Al)O catalysts inhibited the deactivation even after four-cycled DSSO. This can be interpreted by the formation of noble metal-Ni alloys on the surface of Ni particles, and the hydrogen spillover effect of noble metal or noble metal-Ni alloy significantly enhanced the reducibility of Ni particles and the suppression of the oxidation [61,62]. Moreover, alloying Ni with trace noble metals has also been reported to be effective to increase the performance of Ni catalysts in oxidative steam reforming of methane in various aspects such as activity, resistance to Ni oxidation, suppression of hot-spot formation and resistance to coke deposition [42–51]. The effect of noble metals such as Pt, Ru, Rh, and Pd has been investigated on $Ni/CeO_2/Al_2O_3$ catalyst in the pyrolysis + reforming of cedar wood [13,14]. Pt was found to be the most effective additive to enhance the catalytic performance and this can be explained by the Pt-Ni alloy formation. In contrast, the effect of Pd, Ru, and Rh addition to $Ni/CeO_2/Al_2O_3$ catalyst was not so effective and this behavior can be explained by the result that Pd, Ru and Rh species interacted with CeO_2 rather than Ni.

In this work, the Ni catalyst prepared from hydrotalcite-like compounds containing Ni, Mg, and Al by the calcination and reduction, which has been reported to be effective to the steam reforming of biomass tar, was used as a reference catalyst. The modification of the Ni catalyst with a trace of noble metals was attempted in order to develop the catalyst for the oxidative steam reforming of the tar. We optimized a noble metal component and the additive amount of the noble metal. The catalyst was characterized and the relation is discussed between the characterization results and the catalytic performances in oxidative steam reforming of tar.

2. Experimental

2.1. Catalyst preparation

A hydrotalcite-like compound containing Ni, Mg and Al was prepared by co-precipitation method as described previously [60]. An aqueous solution containing the nitrates of Ni^{2+}, Mg^{2+}, and Al^{3+} (Wako Pure Chemical Industries, Ltd.) was dripped slowly into a beaker containing an aqueous solution of sodium carbonate under stirring at room temperature. Simultaneously, an aqueous solution of sodium hydroxide (2 M) was dripped into the beaker to maintain the pH at 10 ± 0.5. The resulting suspension was then kept at room temperature for 24 h. The resulting precipitate was filtered, washed several times with deionized water and dried at 383 K for one night. The resultant was ground to fine powders and calcined at 1073 K for 5 h in a static air atmosphere to give Ni/Mg/Al mixed oxide powder. The molar ratio of Ni/Mg/Al was 9/66/25 and the amount of Ni corresponded to 12 wt%.

Noble metals (Pd, Pt, Au, Ru, Rh and Ir) were added to the Ni/Mg/Al mixed oxide powder by the impregnation method. To per gram of Ni/Mg/Al powder 5 ml aqueous solution of noble metal precursors ($PdCl_2$, $H_2PtCl_6{\cdot}6H_2O$, $HAuCl_4{\cdot}4H_2O$, $RuCl_3{\cdot}nH_2O$, $RhCl_3{\cdot}3H_2O$, and H_2IrCl_6) was dripped for 1 h at room temperature, followed by evaporation of water in air at 343 K and drying at 383 K for one night. The samples were ground to fine powders and calcined at 1073 K for 5 h in a static air atmosphere again. The obtained material was pressed to a disk, crushed and sieved to particles with 30–60 mesh size (Φ 0.3–0.6 mm). The loading amount of Pd was 0–0.5 wt% and the molar ratio of Pd/Ni was 0–0.023. The loading amount of other noble metal was set to the molar ratio of noble metal/Ni = 0.0023. Catalysts in this work are denoted as *x*PdNi, where *x* means the weight percentage of Pd to total weight of the catalyst.

2.2. Biomass

Cedar wood (ground to about 0.1–0.3 mm in size) was used as the biomass feedstock for all the experiments. The moisture content of the cedar wood was 7.2%. The dry-based composition by weight was C 50.8%, H 6.0%, N 0.2%, O 41.8%, and ash 1.1%. The elemental analysis of cedar wood was carried out by the Japan Institute of Energy.

2.3. Catalytic reaction

Oxidative steam gasification of biomass was conducted using a laboratory-scale continuous feeding dual-bed reactor under atmospheric pressure. The scheme of the reactor was similar to that in our previous report and is shown in supporting information (Fig. S1) [11]. The biomass was introduced into the primary bed, and pyrolyzed to form gaseous and solid products at the reaction temperature which was measured by the thermocouple located at the outside of the reactor. The solid product, which is called char, was accumulated in the primary bed. Steam was supplied by a syringe pump into the primary bed. The gaseous products mainly composed of volatile tar, H_2, CO, CO_2, and CH_4 were introduced to the secondary catalyst bed together with steam and carrier gas N_2. Oxygen was introduced near the inlet of catalyst bed during the oxidative steam reforming by a thin tube which was also used for determination of coke amount [11].

The activity tests were carried out at 773 K. The amount of the catalyst used was 0.3 g. The catalyst was reduced with H_2/N_2 (30/30 ml/min) mixed gas at 1073 K for 0.5 h, and these conditions were the same as the ones optimized for 0PdNi catalyst [60]. The reduction gas was purged with N_2 (60 ml/min (2.5 mmol/min)), and then biomass (60 mg/min), water (555 μmol/min), and oxygen (0, 350 or 555 μmol/min) were further fed to the reactor in order to start the activity test. The molar ratio of feeding rate of externally-added O_2 /feeding rate of externally-added steam/feeding rate of carbon in the biomass is represented by ex-O_2/ex-H_2O/C in each experimental result. The effluent gas went through an iced water

condenser in order to remove any solid and liquid species contained in the product gas. The flow rate of the effluent gas was then measured by a soap membrane flow meter. In addition, gas samples were taken at regular time intervals by a syringe and analyzed by gas chromatography. The concentrations of CO, CO_2, and CH_4 were determined by flame ionized detector equipped with a methanator using a stainless steel column packed with Gasukuropack 54. The concentration of H_2 was determined by thermal conductivity detector using stainless steel column packed with a molecular sieve 13X. The formation rates of CO, CH_4, H_2 and CO_2 were calculated from the concentration and the flow rate of the effluent gas. Conversion, which represents carbon-based conversion to gaseous products, was calculated from the feeding rate of biomass and formation rate of $CO + CH_4 + CO_2$. In order to determine the amount of the deposited coke on the catalyst bed and the char accumulated in the primary bed, we stopped the feeding of biomass, steam and oxygen after 15 min of reaction, and then the reactor was purged with N_2. Oxygen was introduced into the secondary and then primary bed at 873 K for the analysis of coke and char, respectively. The amount of CO_2 and CO was analyzed by the gas chromatograph in a similar way to the case of the activity test. The details of the method for determining coke and char amount have also been described in our previous report [11] and the supporting information (Fig. S1). The carbon-based yield of CO, CO_2, CH_4, coke, and char was estimated by the amount of each product to the total carbon in fed biomass. On the other hand, it is difficult to measure the residual tar amount precisely because tar is easily condensed in the reactor system and a part of tar cannot be collected. The tar yield was estimated by subtraction of gaseous and solid carbon-contained product yields from the total carbon in fed biomass, i.e., the yield of tar (%) is defined as (100 – CO yield (%) – CH_4 yield (%) – CO_2 yield (%) – coke yield (%) – char yield (%)). In addition, the formation rates of combustible gases ($CO + H_2 + 4CH_4$) are compared on various tests. Here, the factor for CH_4 is based on the assumption that one CH_4 molecule is formed from one CO and three H_2 molecules by CO hydrogenation ($CO + 3H_2 \rightarrow CH_4 + H_2O$). Furthermore, in order to evaluate the catalyst stability, oxidative steam reforming of tar was carried out under ex-O_2/ex-H_2O/C = 0.24/0.24/1 at 873 K for 120 min using 0.3 g catalysts. After these stability tests, the reactor was purged with N_2 and cooled to room temperature. The spent catalysts were taken out of the catalyst bed and characterized.

2.4. Catalyst characterization

Catalysts were characterized by means of BET surface area measurement, temperature-programmed reduction (TPR), temperature-programmed oxidation (TPO), powder X-ray diffraction (XRD), H_2 chemisorption, transmission electron microscopy (TEM), and extended X-ray absorption fine structure (EXAFS). We characterized catalysts separately after calcination, reduction pretreatment, and catalytic use.

The measurement of BET surface area was conducted on a Micromeritics Gemini 2360.

The TPR profiles were obtained using a fixed-bed flow reactor. The sample weight was about 50 mg and the sample was pretreated in oxygen flow at 773 K for 0.5 h. The temperature was increased from room temperature to 1273 K with a step of 10 K/min and was maintained at 1273 K for 0.5 h under a flow of 30 ml/min 5.0% H_2/Ar. The consumption of H_2 was monitored continuously with TCD gas chromatograph equipped with a frozen acetone trap in order to remove H_2O from the effluent gas.

The reduction degree of Ni in the catalysts after the reduction was determined by TPO measurements. About 50 mg of the reduced catalyst was reduced in the same conditions as those for the reaction tests (with H_2/N_2 ($v/v = 1$) mixed gas at 1073 K for 0.5 h). The sample was transferred to the measurement system under air, and the TPO profile was recorded from room temperature to 1073 K at a heating rate of 10 K/min under a flow of 30 ml/min 1.0% O_2/He. The consumption of O_2 was monitored continuously with TCD gas chromatograph. It should be noted that the total oxygen consumption amount does not include the O_2 adsorption at room temperature, presumably about dispersion values (5–10% of total Ni).

XRD patterns of the samples were measured on a Rigaku MiniFlex 600 diffractometer under air using Cu Kα radiation ($\lambda = 0.154$ nm) generated at 40 kV and 20 mA.

H_2 chemisorption experiments were carried out in a high-vacuum system by volumetric methods. The sample weight of reduced sample was about 150 mg. The catalysts were firstly reduced similarly in the case of TPO measurements. The sample was transferred to the measurement cell under air, and then it was treated with H_2 at 773 K for 1 h to reduce the oxidized surface formed by the contact with air. The re-reduced sample was evacuated at 723 K for 1 h and cooled. The H_2 adsorption was performed at room temperature (297 ± 3 K). Gas pressure at adsorption equilibrium was about 1.1 kPa. The dead volume of the apparatus was about 40 cm^3.

TEM images were taken by means of HD-2700 (Hitachi High-Technologies Co.) equipment operated at 200 kV. The catalysts were crushed to fine powders, dispersed in ethanol by supersonic waves, and deposited on a Cu grid with a holey carbon film under air atmosphere.

EXAFS spectra were measured at the BL01B1 station in the SPring-8 with the approval of the Japan Synchrotron Radiation Research Institute (JASRI) (Proposal No. 2014A1119). The storage ring was operated at 8 GeV. A Si (111) single crystal was used to obtain a monochromatic X-ray beam. For Pd *K*-edge EXAFS, the ion chamber filled with Ar was used as the detector for I_0. For Ni *K*-edge EXAFS, two ion chambers filled with N_2 and 15% Ar diluted with N_2 were used as the detectors for I_0 and I, respectively. The reduced catalysts were pressed into self-supporting 10-mm-diameter wafers under atmosphere, followed by the treatment with H_2 at 773 K for 0.5 h in the cell. After this pretreatment, each sample was transferred to the measurement cell using a glove bag filled with nitrogen to prevent exposure of the sample disk to air. Thickness of the sample for Pd *K*-edge EXAFS was 8 mm and the Pd *K*-edge EXAFS data were collected in a fluorescence mode using Lytle detector at room temperature. Thickness of the sample for Ni *K*-edge EXAFS was 0.4 mm and the Ni *K*-edge EXAFS data were collected in a transmission mode at room temperature and the edge jump was about 2.0. For the analysis of EXAFS spectra, the oscillation was first extracted from the EXAFS data by a spline smoothing method [63]. The oscillation was normalized by the edge height around 50 eV. The Fourier transformation of the k^3-weighted EXAFS oscillation from k space to r space was performed over the range of 30–130 nm^{-1} to obtain a radial distribution function. The inversely Fourier filtered data were analyzed by a usual curve fitting method [64]. For the curve fitting analysis, the empirical phase shift and amplitude functions for the Pd—Pd, Ni—Ni and Ni—O bonds were extracted from the data of Pd foil, Ni foil, and NiO, respectively. Theoretical functions for the Pd—Ni and Ni—O—Mg (or Al) were calculated using the FEFF 8.2 program [65]. The analysis of EXAFS data was performed using the "REX2000" program (Rigaku Co. Version: 2.6). Error bars for each parameter were estimated by stepping each parameter, while optimizing the others parameter, until the residual factor became two times as its minimum value [66].

In order to determine the coke deposition on the catalysts after the stability tests, thermogravimetry-differential thermal analysis (TG-DTA) was conducted with Thermo Plus EVO-II TG-DTA (Rigaku Corp.) at a heating rate of 10 K min^{-1} under an air flow (50 ml min^{-1}) using 10 mg of sample.

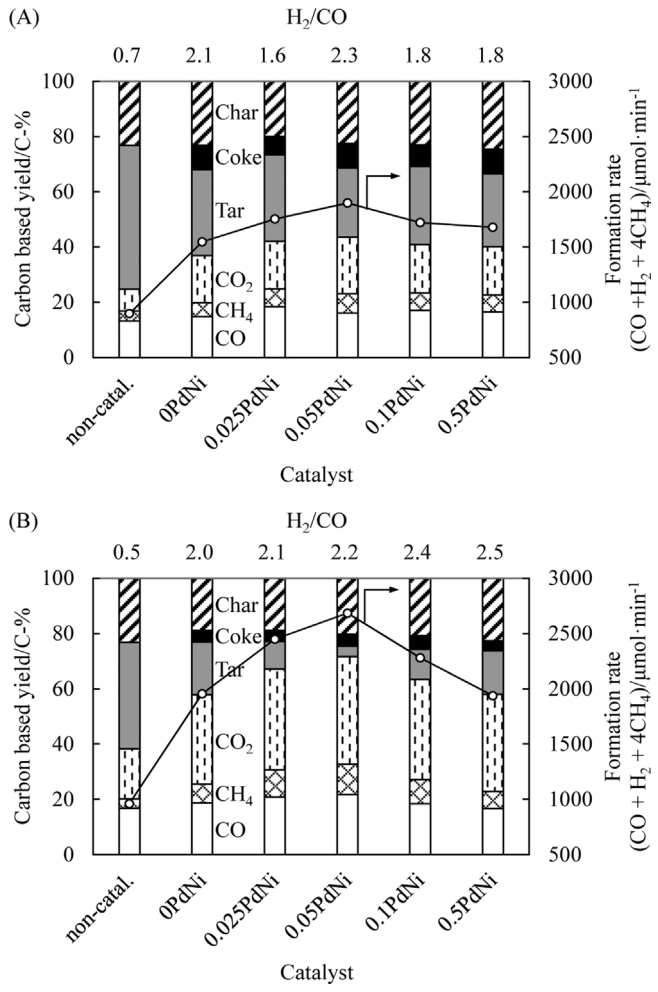

Fig. 1. Effect of Pd amount on the catalytic performance over *x*PdNi catalysts in steam reforming (A) and oxidative steam reforming (B) of tar from cedar pyrolysis. Reaction conditions: biomass 60 mg/min (H_2O 7.2%, C 2356 μmol/min, H 3325 μmol/min, O 1454 μmol/min); molar ratio ex-O_2/ex-H_2O/C: (A) 0/0.24/1 and (B) 0.16/0.24/1; N_2 60 ml/min; reaction temperature 773 K; reaction time 15 min; catalyst 0.3 g. Reduction conditions: 1073 K, H_2/N_2 (30/30 ml/min), 30 min.

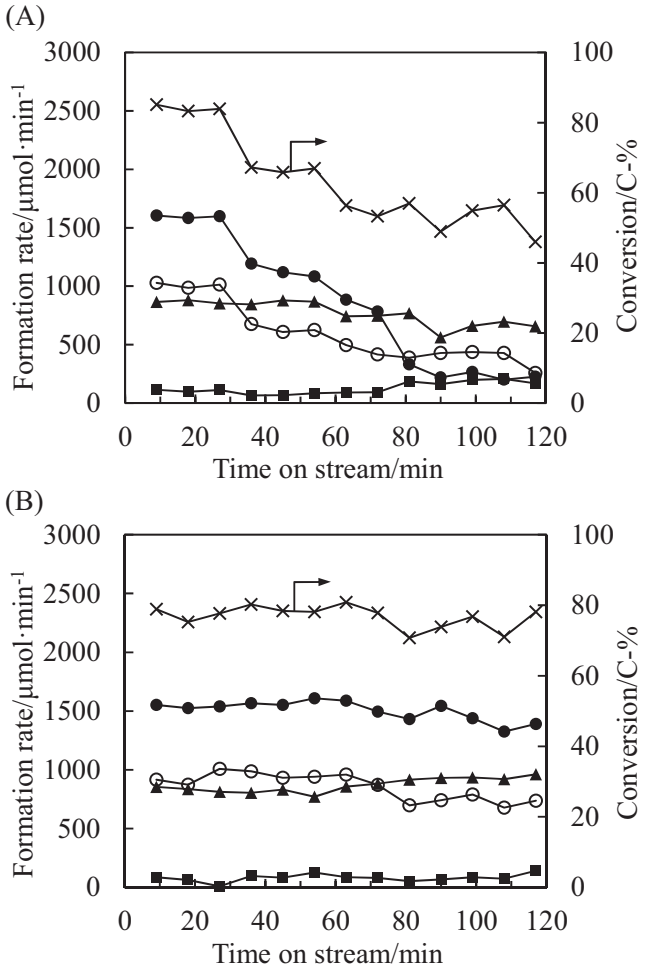

Fig. 2. Reaction time dependence of formation rate of CO, CO_2, CH_4 and H_2 and carbon-based conversion to gaseous products (CO, CO_2 and CH_4) in the oxidative steam reforming of tar over 0PdNi (A) and 0.05PdNi (B) catalysts (×-conversion, ●-H_2, ○-CO, ▲-CO_2, ■-CH_4). Reaction conditions: biomass 60 mg/min (H_2O 7.2%, C 2356 μmol/min, H 3325 μmol/min, O 1454 μmol/min); ex-O_2/ex-H_2O/C = 0.24/0.24/1; N_2 60 ml/min; reaction temperature 873 K; catalyst 0.3 g. Reduction conditions: 1073 K, H_2/N_2 = 30/30 ml/min, 30 min.

3. Results and discussion

3.1. Catalytic performance in steam reforming and oxidative steam reforming of tar from cedar pyrolysis

Fig. 1 shows the effect of Pd amount on the catalytic performance over *x*PdNi (*x* = 0–0.5) catalysts in steam reforming and oxidative steam reforming. Strong addition effect of Pd was observed and the effect was more significant in the oxidative steam reforming than the case in the steam reforming. It has been reported that the activity of Pd itself in the steam reforming of biomass tar [14] or hydrocarbons such as methane [67–69] is not so high as that of monometallic Ni catalysts. Therefore, the contribution of Pd to the steam reforming of tar can be small considering the low activity of Pd itself and the much smaller amount of Pd than Ni. The promoting effect is influenced by the Pd amount and *x* = 0–0.5 (wt%) was determined to be the optimum additive amount. As a result, 0.05PdNi exhibited high formation rate of $CO + H_2 + 4CH_4$ and small amount of residual tar, which represents high performance in oxidative steam reforming. Fig. S2 shows the results of the activity tests of various bimetallic Ni catalysts in steam reforming and oxidative steam reforming of tar. Totally, it was found that the addition of small amount of noble metals was clearly effective in the oxidative steam reforming, and 0.05PdNi showed the highest performance among noble-metal-added catalysts with the same noble metal/Ni molar ratio (0.0023). In addition, we also verified that 0.05PdNi was more effective than Ni-Fe and Ni-Cu catalysts, which have been reported to be effective in steam reforming of tar [23]. Another important point is that the amount of coke deposited on the catalyst surface, which should be as small as possible for the catalyst life, was clearly smaller in the oxidative steam reforming than that in the cases of the steam reforming over all the catalysts. Reaction temperature dependence of the performance of 0.05PdNi and 0PdNi catalysts in the steam reforming and the oxidative steam reforming of the tar was investigated (Fig. S3). At high temperature such as 873 K, the difference in the catalyst performance between 0.05PdNi and 0PdNi became smaller because the residual tar amount became smaller. At lower reaction temperature, it is clear that the 0.05PdNi catalyst gave higher formation rate of $CO + H_2 + 4CH_4$ and smaller amount of the residual tar than the 0PdNi catalyst in the oxidative steam reforming. Fig. 2 shows the reaction time dependence of formation rate and carbon-based conversion to gaseous products in the oxidative steam reforming of tar over 0PdNi and 0.05PdNi catalysts. On the monometallic Ni catalysts (0PdNi), the formation rate of CO, CO_2 and CH_4 decreased gradually and the H_2 formation rate decreased with the reaction

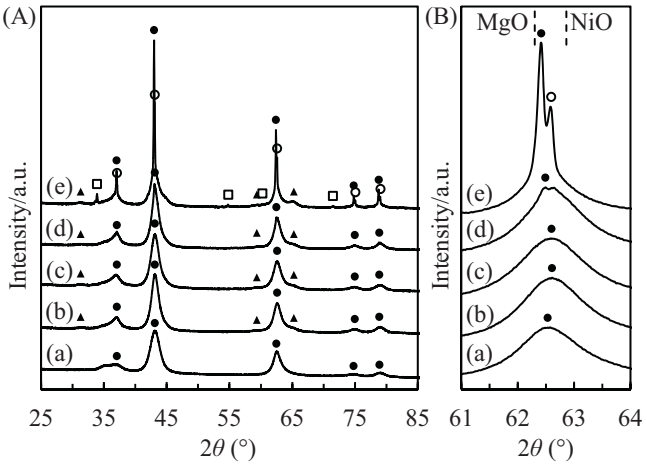

Fig. 3. XRD patterns of *x*PdNi catalysts after calcination at 1073 K. (a) 0PdNi, (b) 0.025PdNi, (c) 0.05PdNi, (d) 0.1PdNi, and (e) 0.5PdNi. Crystalline phases: (●) Mg(Ni, Al)O periclase, (▲) $Mg(Ni)Al_2O_4$ spinel, (◯) Ni-rich Mg(Ni, Al)O, and (□) PdO.

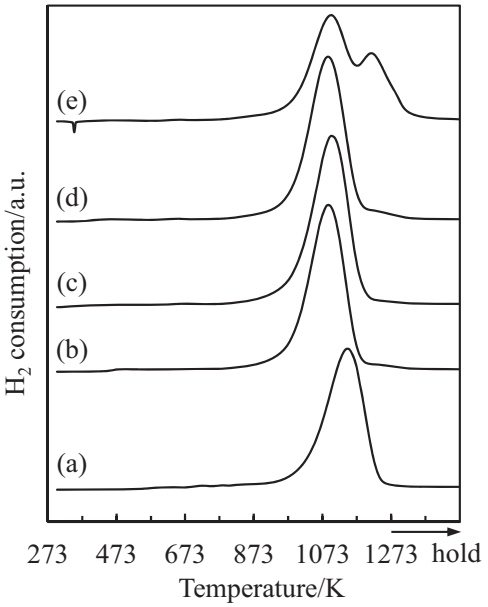

Fig. 4. Temperature programmed reduction profiles of *x*PdNi catalysts after calcination at 1073 K. (a) 0PdNi, (b) 0.025PdNi, (c) 0.05PdNi, (d) 0.1PdNi, and (e) 0.5PdNi. Conditions: 5% H_2/Ar, 30 ml/min; room temperature to 1273 K by 10 K/min, and the temperature was maintained at 1273 K for 30 min; sample weight 50 mg.

time more significantly than the formation rate of other gaseous products, which is connected to low H_2/CO ratio in the product gas. As shown in Fig. 1, the low H_2/CO ratio was observed in the results of non-catalyst, indicating that the 0PdNi catalyst can lose the reforming activity by the catalyst deactivation. In contrast, it is found that the 0.05PdNi catalyst exhibited stable performance for 120 min, indicating the much higher stability of the 0.05PdNi catalyst than the 0PdNi catalyst. The amount of the deposited coke on the catalysts after 120 min reaction was measured by TG-DTA analysis. In the profile of TG-DTA (Fig. S4), the exothermic weight loss at 573–873 K was observed, and the coke amount on 0.05PdNi and 0PdNi catalysts was determined to be 1.4 wt% and 4.0 wt%, respectively. According to our previous report [60], the same Ni catalyst as 0PdNi (with the same composition; a different lot) maintained high activity in the steam reforming of tar with the same reactor under the conditions of ex-H_2O/C = 0.5 and 923 K even after the coke deposition amount reached 3.8 wt%. The deposited coke is mainly filamentous one which is generally less likely to contribute to the catalyst deactivation. The coke amount on 0PdNi in these reactions was similar, and this suggests that the main cause of the catalyst deactivation of 0PdNi in this case is not the coke deposition.

3.2. Catalyst characterization of fresh catalysts

Fig. 3 shows XRD patterns of the *x*PdNi (*x* = 0–0.5) catalysts after the calcination at 1073 K. Broad peaks were observed similarly on all *x*PdNi catalysts except 0.5PdNi and the patterns are similar to those in the previous reports for HTlcs-derived Ni catalysts [60]. Very sharp diffraction peaks were observed on 0.5PdNi catalyst. Table 1 lists the BET surface area of these calcined samples. The BET surface area of 0.5PdNi was clearly smaller than those of other catalysts (Table 1), and this behavior is connected to the sharp XRD peaks on 0.5PdNi. The peaks around $2\theta = 62–63^\circ$ can be assigned to MgO periclase-like solid solution phase containing Al^{3+} and Ni^{2+} [60], which is designated as Mg(Ni,Al)O. On 0.5PdNi catalyst, two peaks were observed at $2\theta = 62.41^\circ$ and 62.58°. Based on the diffraction angle of MgO ($2\theta = 62.30^\circ$) and NiO ($2\theta = 62.86^\circ$), it is interpreted that Mg(Ni, Al)O phases with different Ni concentration were formed [70], and Mg(Ni, Al)O giving high diffraction angle can be assigned to the formation of Ni rich Mg(Ni, Al)O periclase, which may be due to the preparation conditions of higher Pd loading.

It has been known that the addition of Pd enhances the reducibility of Ni catalysts [51]. In order to evaluate the catalyst reducibility, TPR profiles were obtained. On the TPR profile of the 0PdNi catalyst (Fig. 4(a)), the peak due to the reduction of Ni^{2+} species from Mg(Ni, Al)O periclase to Ni^0 appeared as a single broad peak at around 1145 K. The reduction degree of Ni can be calculated from H_2 consumption amount in all the temperature range and the calculated values are also listed in Table 1. It is clear that the H_2 consumption peak on *x*PdNi (*x* = 0.025–0.1) shifted toward lower temperature than that on the 0PdNi catalyst, and the reduction degree was increased by the addition of Pd (Fig. 4(b–d)). The TPR pattern became much different when the Pd loading amount was further increased: Another H_2 consumption peak at higher temperature appeared on 0.5PdNi, and a negative peak was observed at around 363 K (Fig. 4(e)). As mentioned above, 0.5PdNi catalyst has larger size of the oxide crystallites (Fig. 3(e)) and lower surface area (Table 1; calcined state), and these properties can be connected to low reducibility of 0.5PdNi. The negative peak can be assigned to the decomposition of Pd hydride [71], and this indicates the presence of Pd metal. On the other hand, no negative peak was present on *x*PdNi (*x* = 0.025–0.1), which suggests the absence of monometallic Pd particles. The conditions for the reduction pretreatment of the 0PdNi catalyst have already been optimized to obtain better activity and stability in our previous study [60]. Smaller Ni particles are formed with the optimized conditions (1073 K, diluted H_2 with N_2); however, some of Ni^{2+} species remains in the oxide phase. The reduction conditions for *x*PdNi catalysts were set to these conditions. In order to evaluate the reduction degree on the catalysts after the reduction pretreatment, TPO of reduced catalysts was carried out (Fig. 5). The O_2 consumption was observed in wide temperature range (300–800 K), and this is mainly due to the oxidation of Ni^0 to Ni^{2+}. The reduction degree was calculated on this O_2 consumption and the values are also listed in Table 1. The reduction degree from the TPO profiles was smaller than that from TPR profiles because the reduction pretreatment temperature (1073 K) was lower than the highest temperature for the TPR experiment (1273 K). The highest reduction degree was observed on 0.05PdNi. Another important point is that the O_2 consumption at lower temperature than about 500 K on *x*PdNi (*x* = 0.025–0.5) catalysts was larger than that on the 0PdNi catalyst. One possible interpretation is that the presence of Pd accelerated the oxidation of Ni in the Pd-Ni bimetallic system,

Table 1
Physicochemical properties of *x*PdNi catalysts.

Catalysts	Pd/Ni molar ratio/%	BET ($m^2\ g_{cat}^{-1}$)		Particle size of support[c] (nm)	Reduction degree (%)		XRD[f]		H_2 adsorption[g] ($\mu mol\ g_{cat}^{-1}$)	H_2 uptake[h]		TEM[i]	
		Calcined[a]	Reduced[b]		TPR[d]	TPO[e]	*d* (nm)	*D* (%)		*d* (nm)	*D* (%)	*d* (nm)	*D* (%)
0PdNi	0	112	141	11.9	83.2	66.4	10.5	9.2	39.2	16.5	5.9	17.0	5.7
0.025PdNi	0.11	98	109	15.3	93.9	68.3	8.3	11.7	64.6	10.5	9.3	13.1	7.4
0.05PdNi	0.23	91	85	19.7	97.4	71.9	7.1	13.7	81.4	8.8	11.1	10.3	9.4
0.1PdNi	0.46	93	99	17.0	96.9	61.9	6.5	14.9	75.8	8.1	12.0	9.7	10.0
0.5PdNi	2.30	73	88	19.0	91.1	38.4	5.9	16.5	56.6	6.7	14.4	8.0	12.1

[a] Calcination of hydrotalcite-like compounds at 1073 K for 5 h in the catalyst preparation.
[b] Reduction of the calcined samples in H_2/N_2 (30/30 ml/min) at 1073 K for 30 min.
[c] Calculated using the BET surface areas of the reduced samples, assuming that cubic structure with uniform size.
[d] Assuming the stoichiometry of the reduction of $Ni^{2+} + H_2 \rightarrow Ni^0 + 2H^+$ and all H_2 consumption is due to the reduction of Ni species and the contribution of Pd is neglected because the amount of Pd was much smaller than Ni (Fig. 4).
[e] Assuming the stoichiometry of the oxidation of $Ni^0 + 1/2O_2 \rightarrow Ni^{2+} + O^{2-}$ and all the O_2 consumptions in the range of 273–1073 K is due to the oxidation of Ni metal on the samples after reduction pretreatment at 1073 K using H_2/N_2 (30/30 ml/min) for 30 min, and the contribution of Pd is neglected because of the much smaller amount of Pd compared to Ni (Fig. 5).
[f] Particle size *d* was calculated from the full width at half maximum of the Ni (2 0 0) reflection peak at $2\theta \approx 51.8^\circ$ in the XRD using the Scherrer equation [75,76] and the Scherrer constant is 0.9. Dispersion of Ni metal particles *D*% = 9.71/(particle size *d* (nm) calculated by XRD data) × 10 (Fig. 6) [77].
[g] Total adsorption of H_2 (reversible + irreversible adsorption) at room temperature.
[h] Particle size *d* (nm) = 9.71/(dispersion (%) calculated by total H_2 adsorption) × 10 [77]. Dispersion of Ni metal particles *D*% = 2 × (H_2 uptake (mol))/(the reduction degree from TPO × Ni loading (mol) + Pd loading (mol)) × 100%, assuming H/(Ni or Pd) = 1.
[i] Particle size *d* (nm) = $\sum n_i d^3 / \sum n_i d^2$. Dispersion of Ni metal particles *D*% = 9.71/(particle size *d* (nm) obtained from TEM observation) × 10 [77].

because of higher ability of Pd in oxygen activation than that of Ni [72,73]. It should be noted that a negative peak was observed at around 987 K on 0.5PdNi catalyst (Fig. 5(e)), which can be assigned to the thermal decomposition of PdO ($PdO \rightarrow Pd + 1/2O_2$) [74]. This O_2 formation amount was O/Pd = 0.62 as the molar ratio, which suggests the presence of pure Pd metal species. The presence of Pd metal can be associated with the decomposition of Pd hydride in the TPR profile on 0.5PdNi catalyst.

Fig. 6 shows the XRD patterns of *x*PdNi after the reduction pretreatment. The large peaks were also assigned to Mg(Ni, Al)O similarly to the cases of the catalysts after calcination (Fig. 3). A different point is that the peaks due to Ni metal appeared on the catalyst after the reduction. The new diffraction peaks were observed at $2\theta \approx 44.5^\circ$, 51.8°, and 76.3°, corresponding to the (1 1 1), (2 0 0), and (2 2 0) reflections, respectively, of Ni metal (JCPDS 01-070-1849). It should be noted that no shift of the peaks due to Ni metal was detected (Fig. 6B) on *x*PdNi catalysts. In this case, the molar ratio of Pd to Ni metal was so small that it is difficult to verify the formation of Pd-Ni alloy from the XRD results of *x*PdNi after the reduction pretreatment. On 0.5PdNi (Fig. 6C (e)), relative intensity of the peak due to Ni-rich Mg(Ni, Al)O ($2\theta = 62.56^\circ$) to that due to Mg(Ni, Al)O ($2\theta = 62.39^\circ$) became smaller by the reduction pretreatment, suggesting that Ni species in Ni-rich Mg(Ni, Al)O phase tend to be reduced more preferentially than those of Mg(Ni, Al)O. In addition, the peaks assigned to Pd metal were detected only on 0.5PdNi after the reduction pretreatment (Fig. 6(e)), and this can be associated with the decomposition of Pd hydride in the TPR profile (Fig. 4(e)) and the decomposition of PdO in the TPO profile (Fig. 5(e)) on 0.5PdNi. The particle size of Ni metal was calculated from the peak at $2\theta \approx 51.8^\circ$ [75,76], and the dispersion of Ni metal particles were also calculated on the basis of the particle size [77]. The obtained results of Ni metal particle size and dispersion are also listed in Table 1. It is found that the particle sizes of Ni metal particles decreased gradually with increasing Pd addition amount. Next we also measured the amount of H_2 adsorption, and the results are also listed in Table 1. The amount of H_2 adsorption increased with increasing Pd amount in the range of $x = 0$–0.05 on *x*PdNi, and this behavior can be explained by the increase of the reduction degree from TPO and decrease of the particle size of Ni by the Pd addition. In contrast, the amount of H_2 adsorption decreased with increasing Pd amount in the range of $x > 0.05$. This tendency can be mainly due to the decrease of the reduction degree in this *x* range. Combined with the reduction degree from TPO, the amount of H_2 adsorption can give the particle size of Ni metal and the dispersion, and the obtained values are also listed in Table 1. Compared to the particle size and the dispersion from XRD, a little larger particle size and lower dispersion were obtained from H_2 adsorption and the reduction degree from TPO, although the dependence of Pd additive amount on particle size is similar in both cases. A possible interpretation is that the surface of Ni metal particles is partially covered by the Mg(Ni, Al)O oxide particles, which have comparable size to the Ni metal particles and interact with Ni metal particles [60]. Table 1 also lists the particles size and the calculated dispersion from TEM observation. TEM images and the distribution of particle size are shown in Fig. 7A and B, Fig. S5, and S6. Although the particle size from TEM was a little larger than that from H_2 uptake and XRD, the

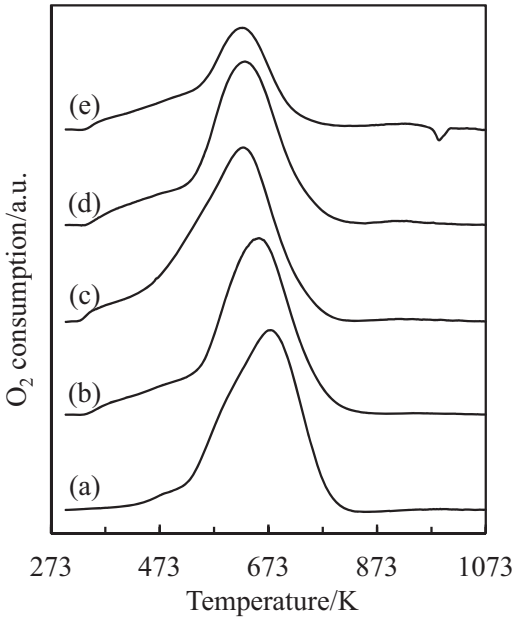

Fig. 5. Temperature programmed oxidation profiles of *x*PdNi catalysts after reduction. (a) 0PdNi, (b) 0.025PdNi, (c) 0.05PdNi, (d) 0.1PdNi, and (e) 0.5PdNi. Conditions: 1% O_2/He, 30 ml min^{-1}; room temperature to 1073 K by 10 K/min; sample weight 50 mg; prereduction H_2/N_2 (30/30 ml/min), 1073 K, 30 min.

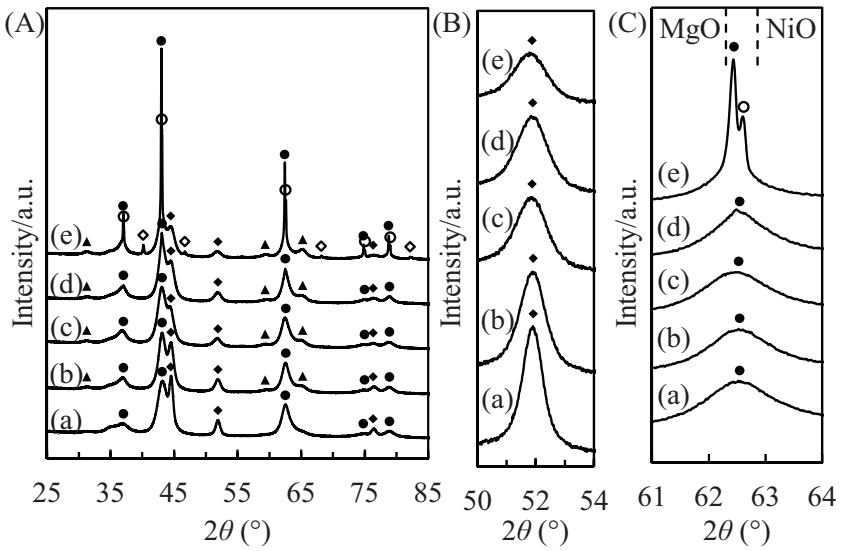

Fig. 6. XRD patterns of the reduced *x*PdNi catalysts. (a) 0PdNi, (b) 0.025PdNi, (c) 0.05PdNi, (d) 0.1PdNi, and (e) 0.5PdNi. Crystalline phases: (●) Mg(Ni, Al)O periclase, (○) Ni-rich Mg(Ni, Al)O, (▲) Mg(Ni)Al_2O_4 spinel, (♦) Ni metal, and (◊) Pd metal. Reduced at 1073 K in H_2/N_2 (30/30 ml/min) for 30 min.

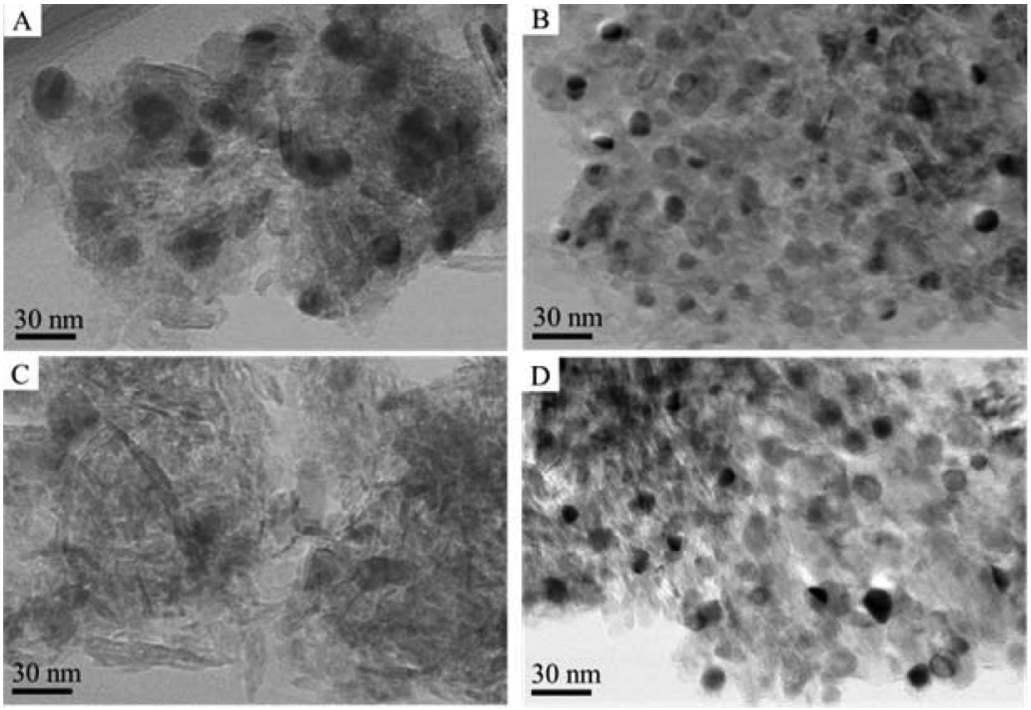

Fig. 7. TEM images of 0PdNi and 0.05PdNi after reduction and after 2 h stability test. (A) 0PdNi after reduction, (B) 0.05PdNi after reduction, (C) 0PdNi after reaction (Fig. 2A), and (D) 0.05PdNi after reaction (Fig. 2B). Treatment conditions: (A, B) reduction, H_2/N_2 = 30/30 ml/min, 1073 K, 0.5 h; (C, D) stability test, as the same as that in Fig. 2.

tendency regarding the amount of Pd addition was similar to that from other methods.

In order to evaluate the interaction between Pd and Ni, Pd *K* edge and Ni *K*-edge EXAFS analyses were carried out. Fig. 8 shows the results of the Pd *K*-edge EXAFS analysis of 0.05PdNi after reduction and the curve fitting results are listed in Table 2. Only Pd-Ni bond is present and the bond length is determined to be 0.253 nm, which is clearly shorter than that of Pd-Pd bond (0.275 nm) in Pd foil and is comparable to that of Ni-Ni bond (0.249 nm) in Ni foil. This bond length agreed well with that reported previously [50,69]. The coordination number of the Pd-Ni bond is determined to be 5.7 ± 0.8, which is much smaller than that of the bulk atom in fcc metal (12). The bond length and the coordination number suggest that Pd atoms are isolatedly located in the surface layer of Ni metal particles. Fig. 9 shows the results of Ni *K*-edge EXAFS analysis and the curve fitting results are summarized in Table 3. Ni—Ni, Ni—O, and Ni—O—Mg(Al) bonds are present. The bond length of the Ni-Ni bond (0.249 nm) in 0.05PdNi is the same as that in Ni foil, and this bond is assigned to the bond in Ni metal particles. The bond length of Ni—O (0.203 nm) and Ni—O—Mg(or Al) (0.294 nm) bond are close to those of Mg—O bond (0.212 nm) and Mg—O—Mg bond (0.300 nm) in MgO [78], respectively, indicating that Ni—O and Ni—O—Mg bonds can be assigned to the Ni ion species in Mg(Ni, Al)O solid solution. The coordination number of Ni—O in the bulk of Mg(Ni, Al)O solid solution is 6.0. Using this bulk coordination number of Ni—O and considering the relatively large particle size of Mg(Ni, Al)O, it is

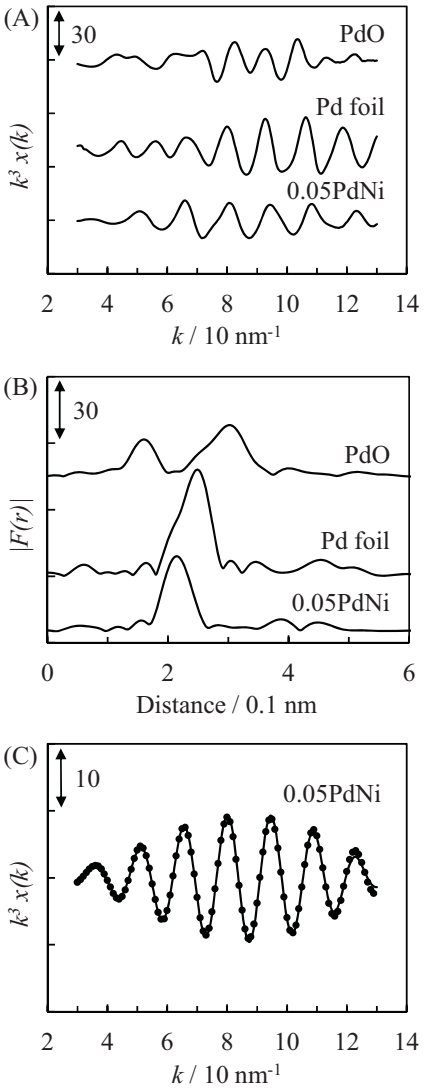

Fig. 8. Results of the Pd *K*-edge EXAFS analysis of 0.05PdNi after reduction and reference compounds. (A) k^3-weighted EXAFS oscillations, (B) Fourier transform of k^3-weighted Pd *K*-edge EXAFS (FT range: 30–130 nm^{-1}), and (C) Fourier filtered EXAFS data (solid line) and calculated data (dotted line) (FF range: 0.1803–0.2915 nm).

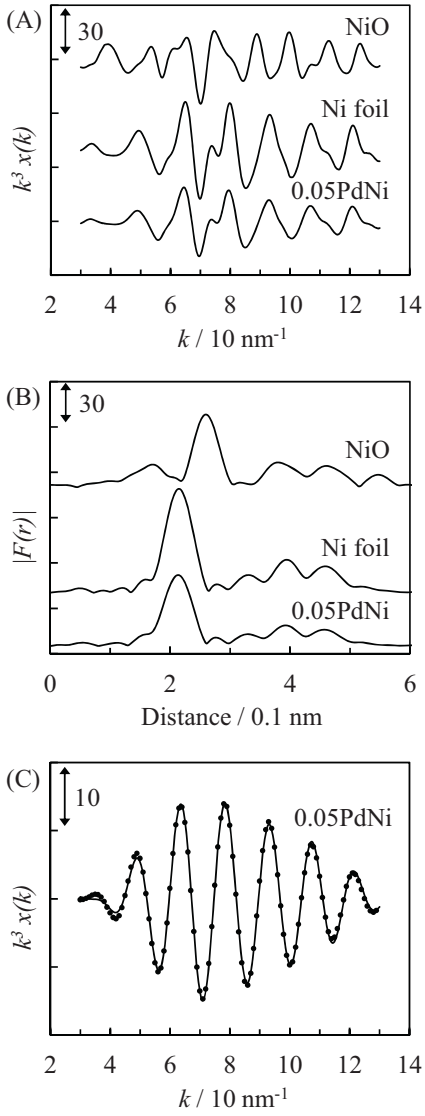

Fig. 9. Results of the Ni *K*-edge EXAFS analysis of 0.05PdNi after reduction and reference compounds. (A) k^3-weighted EXAFS oscillations, (B) Fourier transform of k^3-weighted Ni *K*-edge EXAFS (FT range: 30–130 nm^{-1}), and (C) Fourier filtered EXAFS data (solid line) and calculated data (dotted line) (FF range: 0.1113–0.3068 nm).

possible to estimate the reduction degree of Ni from the coordination number (1.8) of Ni—O in 0.05PdNi. This reduction degree from EXAFS analysis is calculated to be 70% ((6–1.8)/6), which agreed well with that from TPO analysis (Table 1). In addition, it is also possible to estimate the coordination number of Ni metal particles excluding the contribution of Ni ionic species in Mg(Ni, Al)O. It is calculated to be 12 (=8.4/0.7), suggesting that the size of Ni metal particles is large, which is also supported by the determination of Ni particles size from other techniques.

The order of catalytic activity of *x*PdNi catalyst in Fig. 1B well accorded with the order of the amount of H_2 adsorption. The large amount of H_2 adsorption on 0.05PdNi can be caused by the simultaneous enhancement of the reduction degree of Ni species and the dispersion of Ni metal particles by the addition of suitable amount of Pd.

Table 2
Curve fitting results of the Pd *K*-edge EXAFS of 0.05PdNi after reduction.

Entry	Catalyst	Shells	CN[a]	R[b] (10^{-1} nm)	σ[c] (10^{-1} nm)	ΔE_0[d] (eV)	R_f[e] (%)
1	0.05PdNi	Pd-Ni	5.7 ± 0.8	2.53 ± 0.01	0.077 ± 0.005	−1.1 ± 1.6	1.0
2	Pd foil	Pd-Pd	12.0	2.75	0.060	0.0	–

Fourier transform range: 30–130 nm^{-1}. Fourier filtering range: 0.1803–0.2915 nm.
[a] Coordination number.
[b] Bond distance.
[c] Debye–Waller factor.
[d] Difference in the origin of photoelectron energy between the reference and the sample.
[e] Residual factor.

Table 3
Curve fitting results of the Ni *K*-edge EXAFS of 0.05PdNi after reduction.

Entry	Catalyst	Shells	CN[a]	R^b (10^{-1} nm)	σ^c (10^{-1} nm)	$\Delta E_0{}^d$ (eV)	$R_f{}^e$ (%)
1	0.05PdNi	Ni—Ni	8.4 ± 0.4	2.49 ± 0.003	0.061 ± 0.003	−2.1 ± 0.7	0.26
		Ni—O	1.8 ± 0.7	2.03 ± 0.035	0.062 ± 0.029	6.7 ± 6.3	
		Ni—O—Mg(Al)[f]	1.4 ± 0.9	2.94 ± 0.042	0.060 ± 0.055	8.0 ± 4.5	
2	Ni foil	Ni—Ni	12.0	2.49	0.060	0.0	–
3	NiO	Ni—O	6.0	2.09	0.060	0.0	–

Fourier filtering range: 0.1113–0.3068 nm. Fourier transform range: 30–130 nm^{-1}.
[a] Coordination number.
[b] Bond distance.
[c] Debye–Waller factor.
[d] Difference in the origin of photoelectron energy between the reference and the sample.
[e] Residual factor.
[f] It is difficult to distinguish between Mg and Al ions as a backscattering atom.

3.3. Characterization of catalysts after stability test

In oxidative steam reforming reaction, monometallic Ni catalysts tend to be deactivated by the oxidation of Ni species as mentioned in the introduction. In order to elucidate the reason for the deactivation of the 0PdNi catalyst, we characterized the catalysts after the reaction of Fig. 2. Fig. 10 shows the XRD patterns of *x*PdNi (*x* = 0 and 0.05) catalysts after 2 h stability test (Fig. 2). The diffraction peaks of Ni metal totally disappeared from the XRD pattern of the 0PdNi catalyst after the stability test (Fig. 10 (b)). The TEM image of the 0PdNi catalyst after the stability test is shown in Fig. 7C. The Ni metal particles having high contrast were not detected. Both XRD and TEM results of the 0PdNi catalyst indicate that Ni metal particles disappeared, and this can be due to the oxidation of Ni metal particles. In contrast, XRD pattern of 0.05PdNi after the stability test (Fig. 10(a)) was almost the same as that of 0.05PdNi after the reduction pretreatment (Fig. 6(c)). The particle size of 0.05PdNi after the stability test is calculated to be 7.6 nm, which almost agreed with 7.1 nm of 0.05PdNi after the reduction. In addition, there was no apparent change in the TEM images between 0.05PdNi after the stability test (particle size, 10.3 nm, Fig. 7D) and 0.05PdNi after the reduction pretreatment (particle size, 10.1 nm, Fig. 7B). Both XRD and TEM results of 0.05PdNi after the reaction indicate that metal particles are maintained under the conditions of the oxidative steam reforming reaction, and this high resistance to deactivation by the oxidation can be caused by Pd species dispersed on the surface of the Ni metal particles. Similar role of noble metals on the resistance to the oxidation of Ni metal particles by the direct interaction between noble metals and Ni metal has been also reported in the oxidative steam reforming of methane [42–51].

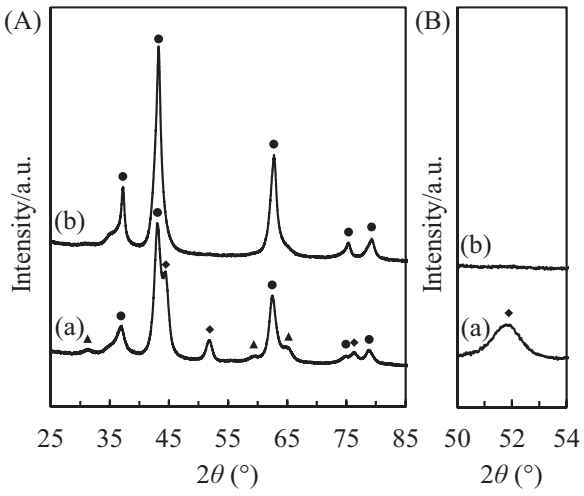

Fig. 10. XRD patterns of the catalysts after stability test (a) 0.05PdNi and (b) 0PdNi. The condition of the stability test was the same as that in Fig. 2. Crystalline phases: (●) Mg(Ni, Al)O periclase, (▲) $Mg(Ni)Al_2O_4$ spinel, and (♦) Ni metal.

4. Conclusions

1. The addition of trace noble metals enhanced the catalytic performances of hydrotalcite-like compounds-derived Ni/Mg/Al catalyst in oxidative steam reforming of biomass tar, and Pd is the most suitable additive when the same molar ratio of noble metal/Ni = 0.0023 was applied.
2. The most suitable addition amount of Pd is 0.05 wt% (in the range of 0–0.5 wt%; Pd/Ni = 0.0023), and the optimized bimetallic 0.05PdNi catalyst shows much higher stability than the monometallic 0PdNi catalyst in the oxidative steam reforming of tar.
3. The addition of 0.05 wt% Pd increases the reduction degree of Ni species and the dispersion of Ni metal particles simultaneously, resulting in the largest H_2 adsorption amount. The large H_2 adsorption amount can be attributed to the highest catalytic performance of 0.05PdNi among *x*PdNi (*x* = 0–0.5) catalysts. The EXAFS analysis indicates that Pd atoms are dispersed isolatedly on the surface of Ni metal particles.
4. Nickel metal particles of monometallic 0PdNi catalyst is totally oxidized after 2 h stability test. In contrast, the oxidation of Ni metal particles is effectively suppressed on bimetallic 0.05PdNi catalyst, resulting from the enhancement of the reducibility by Pd metal atoms on the surface of Ni metal particles.

Acknowledgements

Authors appreciate Technical Division, School of Engineering, Tohoku University for TEM observation of the catalysts. Part of this work is funded by the program of Next-generation Energies for Tohoku Recovery.

Appendix A. Supplementary data

Supplementary data associated with this article can be found, in the online version, at http://dx.doi.org/10.1016/j.apcatb.2015.05.042

References

[1] G.W. Huber, S. Iborra, A. Corma, Chem. Rev. 106 (2006) 4044–4098.
[2] H. de Lasa, E. Salaices, J. Mazumder, R. Lucky, Chem. Rev. 111 (2011) 5404–5433.
[3] M. Asadullah, Renew. Sustain. Energy Rev. 29 (2014) 201–215.
[4] M. Asadullah, Renew. Sustain. Energy Rev. 40 (2014) 118–132.
[5] S.A. Chattanathan, S. Adhikari, N. Abdoulmoumine, Renew. Sustain. Energy Rev. 16 (2012) 2366–2372.
[6] F.L. Chan, A. Tanksale, Renew. Sustain. Energy Rev. 38 (2014) 428–438.
[7] D. Li, Y. Nakagawa, K. Tomishige, Chin. J. Catal. 33 (2012) 583–594.
[8] D. Li, L. Wang, M. Koike, K. Tomishige, J. Jpn. Petrol. Inst. 56 (2013) 253–266.

[9] D. Li, M. Tamura, Y. Nakagawa, K. Tomishige, Bioresour. Technol. 178 (2015) 53–64.
[10] T. Miyazawa, T. Kimura, J. Nishikawa, S. Kado, K. Kunimori, K. Tomishige, Catal. Today 115 (2006) 254–262.
[11] T. Kimura, T. Miyazawa, J. Nishikawa, S. Kado, K. Okumura, T. Miyao, S. Naito, K. Kunimori, K. Tomishige, Appl. Catal. B: Environ. 68 (2006) 160–170.
[12] K. Tomishige, T. Kimura, J. Nishikawa, T. Miyazawa, K. Kunimori, Catal. Commun. 8 (2007) 1074–1079.
[13] J. Nishikawa, T. Miyazawa, K. Nakamura, M. Asadullah, K. Kunimori, K. Tomishige, Catal. Commun. 9 (2008) 195–201.
[14] J. Nishikawa, K. Nakamura, M. Asadullah, T. Miyazawa, K. Kunimori, K. Tomishige, Catal. Today 131 (2008) 146–155.
[15] K. Nakamura, T. Miyazawa, T. Sakurai, T. Miyao, S. Naito, N. Begum, K. Kunimori, K. Tomishige, Appl. Catal. B: Environ. 86 (2009) 36–44.
[16] L. Wang, D. Li, M. Koike, S. Koso, Y. Nakagawa, Y. Xu, K. Tomishige, Appl. Catal. A: Gen. 392 (2011) 248–255.
[17] L. Wang, Y. Hisada, M. Koike, D. Li, H. Watanabe, Y. Nakagawa, K. Tomishige, Appl. Catal. B: Environ. 121–122 (2012) 95–104.
[18] M. Koike, D. Li, Y. Nakagawa, K. Tomishige, ChemSusChem 5 (2012) 2312–2314.
[19] M. Koike, C. Ishikawa, D. Li, L. Wang, Y. Nakagawa, K. Tomishige, Fuel 103 (2013) 122–129.
[20] L. Wang, D. Li, M. Koike, H. Watanabe, Y. Xu, Y. Nakagawa, K. Tomishige, Fuel 112 (2013) 654–661.
[21] D. Li, C. Ishikawa, M. Koike, L. Wang, Y. Nakagawa, K. Tomishige, Int. J. Hydrogen Energy 38 (2013) 3572–3581.
[22] L. Wang, J. Chen, H. Watanabe, Y. Xu, M. Tamura, Y. Nakagawa, K. Tomishige, Appl. Catal. B: Environ. 160–161 (2014) 701–715.
[23] D. Li, M. Koike, L. Wang, Y. Nakagawa, Y. Xu, K. Tomishige, ChemSusChem 7 (2014) 510–522.
[24] L. Wang, D. Li, H. Watanabe, M. Tamura, Y. Nakagawa, K. Tomishige, Appl. Catal. B: Environ. 150–151 (2014) 82–92.
[25] D. Li, M. Koike, J. Chen, Y. Nakagawa, K. Tomishige, Int. J. Hydrogen Energy 39 (2014) 10959–10970.
[26] T. Furusawa, A. Tsutsumi, Appl. Catal. A: Gen. 278 (2005) 207–212.
[27] T. Furusawa, A. Tsutsumi, Appl. Catal. A: Gen. 278 (2005) 195–205.
[28] T. Furusawa, Y. Miura, Y. Kori, M. Sato, N. Suzuki, Catal. Commun. 10 (2009) 552–556.
[29] T. Furusawa, K. Saito, Y. Kori, Y. Miura, M. Sato, N. Suzuki, Fuel 103 (2013) 111–121.
[30] Y. Sekine, D. Mukai, Y. Murai, S. Tochiya, Y. Izutsu, K. Sekiguchi, N. Hosomura, H. Arai, E. Kikuchi, Y. Sugiura, Appl. Catal. A: Gen. 451 (2013) 160–167.
[31] D. Mukai, S. Tochiya, Y. Murai, M. Imori, Y. Sugiura, Y. Sekine, Appl. Catal. A: Gen. 464–465 (2013) 78–86.
[32] D. Mukai, S. Tochiya, Y. Murai, M. Imori, T. Hashimoto, Y. Sugiura, Y. Sekine, Appl. Catal. A: Gen. 453 (2013) 60–70.
[33] K. Takise, M. Imori, D. Mukai, S. Ogo, Y. Sugiura, Y. Sekine, Appl. Catal. A: Gen. 489 (2015) 155–161.
[34] U. Oemar, M.L. Ang, K. Hidajat, S. Kawi, AlChE J. 60 (2014) 4190–4198.
[35] U. Oemar, M.L. Ang, K. Hidajat, S. Kawi, RSC Adv. 5 (2015) 17834–17842.
[36] U. Oemar, M.L. Ang, W.F. Hee, K. Hidajat, S. Kawi, Appl. Catal. B: Environ. 148–149 (2014) 231–242.
[37] J. Ashok, Y. Kathiraser, M.L. Ang, S. Kawi, Appl. Catal. B: Environ. 172–173 (2015) 116–128.
[38] T.M.C. Hoang, N.K. Rao, L. Lefferts, K. Seshan, ChemCatChem 7 (2015) 468–478.
[39] B. Matas Güell, I.V. Babich, L. Lefferts, K. Seshan, Appl. Catal. B: Environ. 106 (2011) 280–286.
[40] M.A. Peña, J.P. Gómez, J.L.G. Fierro, Appl. Catal. A: Gen. 144 (1996) 7–57.
[41] J.R. Rostrup-Nielsen, Catal. Today 71 (2002) 243–247.
[42] K. Tomishige, S. Kanazawa, M. Sato, K. Ikushima, K. Kunimori, Catal. Lett. 84 (2002) 69–74.
[43] K. Tomishige, S. Kanazawa, S.-I. Ito, K. Kunimori, Appl. Catal. A: Gen. 244 (2003) 71–82.
[44] B. Li, S. Kado, Y. Mukainakano, M. Nurunnabi, T. Miyao, S. Naito, K. Kunimori, K. Tomishige, Appl. Catal. A: Gen. 304 (2006) 62–71.
[45] K. Tomishige, J. Jpn. Petrol. Inst. 50 (2007) 287–298.
[46] B. Li, S. Kado, Y. Mukainakano, T. Miyazawa, T. Miyao, S. Naito, K. Okumura, K. Kunimori, K. Tomishige, J. Catal. 245 (2007) 144–155.
[47] Y. Mukainakano, B. Li, S. Kado, T. Miyazawa, K. Okumura, T. Miyao, S. Naito, K. Kunimori, K. Tomishige, Appl. Catal. A: Gen. 318 (2007) 252–264.
[48] K. Yoshida, K. Okumura, T. Miyao, S. Naito, S.-I. Ito, K. Kunimori, K. Tomishige, Appl. Catal. A: Gen. 351 (2008) 217–225.
[49] Y. Mukainakano, K. Yoshida, S. Kado, K. Okumura, K. Kunimori, K. Tomishige, Chem. Eng. Sci. 63 (2008) 4891–4901.
[50] Y. Mukainakano, K. Yoshida, K. Okumura, K. Kunimori, K. Tomishige, Catal. Today 132 (2008) 101–108.
[51] D. Li, Y. Nakagawa, K. Tomishige, Appl. Catal. A: Gen. 408 (2011) 1–24.
[52] K. Tomishige, Y. Himeno, Y. Matsuo, Y. Yoshinaga, K. Fujimoto, Ind. Eng. Chem. Res. 39 (2000) 1891–1897.
[53] H.S. Bengaard, J.K. Nørskov, J. Sehested, B.S. Clausen, L.P. Nielsen, A.M. Molenbroek, J.R. Rostrup-Nielsen, J. Catal. 209 (2002) 365–384.
[54] M. Nurunnabi, Y. Mukainakano, S. Kado, T. Miyazawa, K. Okumura, T. Miyao, S. Naito, K. Suzuki, K.-I. Fujimoto, K. Kunimori, K. Tomishige, Appl. Catal. A: Gen. 308 (2006) 1–12.
[55] S. Li, J. Gong, Chem. Soc. Rev. 43 (2014) 7245–7256.
[56] Y. Matsuo, Y. Yoshinaga, Y. Sekine, K. Tomishige, K. Fujimoto, Catal. Today 63 (2000) 439–445.
[57] K. Tomishige, Y. Matsuo, Y. Yoshinaga, Y. Sekine, M. Asadullah, K. Fujimoto, Appl. Catal. A: Gen. 223 (2002) 225–238.
[58] M. Nurunnabi, Y. Mukainakano, S. Kado, B. Li, K. Kunimori, K. Suzuki, K.-I. Fujimoto, K. Tomishige, Appl. Catal. A: Gen. 299 (2006) 145–156.
[59] F. Cavani, F. Trifirò, A. Vaccari, Catal. Today 11 (1991) 173–301.
[60] D. Li, L. Wang, M. Koike, Y. Nakagawa, K. Tomishige, Appl. Catal. B: Environ. 102 (2011) 528–538.
[61] T. Miyata, D. Li, M. Shiraga, T. Shishido, Y. Oumi, T. Sano, K. Takehira, Appl. Catal. A: Gen. 310 (2006) 97–104.
[62] D. Li, I. Atake, T. Shishido, Y. Oumi, T. Sano, K. Takehira, J. Catal. 250 (2007) 299–312.
[63] J.W. Cook Jr., D.E. Sayers, J. Appl. Phys. 52 (1981) 5024–5031.
[64] K. Okumura, S. Matsumoto, N. Nishiaki, M. Niwa, Appl. Catal. B: Environ. 40 (2003) 151–159.
[65] A.L. Ankudinov, B. Ravel, J.J. Rehr, S.D. Conradson, Phys. Rev. B 58 (1998) 7565–7576.
[66] K. Tomishige, K. Asakura, Y. Iwasawa, J. Catal. 149 (1994) 70–80.
[67] Y.G. Chen, O. Yamazaki, K. Tomishige, K. Fujimoto, Catal. Lett. 39 (1996) 91–95.
[68] B. Li, K. Maruyama, M. Nurunnabi, K. Kunimori, K. Tomishige, Appl. Catal. A: Gen. 275 (2004) 157–172.
[69] M. Nurunnabi, Y. Mukainakano, S. Kado, T. Miyao, S. Naito, K. Okumura, K. Kunimori, K. Tomishige, Appl. Catal. A: Gen. 325 (2007) 154–162.
[70] M. Nurunnabi, B. Li, K. Kunimori, K. Suzuki, K.-I. Fujimoto, K. Tomishige, Appl. Catal. A: Gen. 292 (2005) 272–280.
[71] T. Paryjczak, J.M. Farbotko, K.W. Jóźwiak, React. Kinet. Catal. Lett. 20 (1982) 227–231.
[72] J.T. Stuckless, C.E. Wartnaby, N. Al-Sarraf, St J.B. Dixon-Warren, M. Kovar, D.A. King, J. Chem. Phys. 106 (1997) 2012–2030.
[73] J. Goschnick, M. Wolf, M. Grunze, W.N. Unertl, J.H. Block, J. Loboda-Cackovic, Surf. Sci. 178 (1986) 831–841.
[74] R.J. Farrauto, J.K. Lampert, M.C. Hobson, E.M. Waterman, Appl. Catal. B: Environ. 6 (1995) 263–270.
[75] P. Scherrer, Gött. Nachr. 2 (1918) 98–100.
[76] A.L. Patterson, Phys. Rev. 56 (1939) 978–982.
[77] C.H. Bartholomew, R.B. Pannell, J.L. Butler, J. Catal. 65 (1980) 335–347.
[78] K. Tomishige, Y. Nagasawa, U. Lee, Y. Iwasawa, Bull. Chem. Soc. Jpn. 70 (1997) 1607–1614.